International Forum on Aeroelasticity and Structural Dynamics
IFASD 2019
9-13 June 2019, Savannah, Georgia, USA

A GEOMETRICALLY NONLINEAR FINITE ELEMENT MODEL FOR AEROELASTIC ANALYSIS OF PLATE-LIKE WING AEROSTRUCTURES

Gefferson C. Silva[1], **Mauricio V. Donadon**[1], **Flavio J. Silvestre**[2]

[1]Aeronautical Institute of Technology
São José dos Campos, São Paulo Brazil
geffersonports@gmail.com
donadon@ita.br

[2] Technische Universität Berlin
Berlin, Brandenburg Germany
flavio.silvestre@tu-berlin.de

Keywords: total lagrangian, nonlinear fem, aeroelasticity, modified strip theory

Abstract: This work presents the development of a finite element beam model accounting for structural and aerodynamic nonlinearities regarding large deflections. The total Lagrangian formulation is employed for describing the exact Timoshenko's bending kinematics, whereas the torsion is modeled as an uniform torsion and uncoupled from the bending motion. The aerodynamic description is based on an unsteady 2D strip theory in the time domain with the Jones approximation for Wagner's function. In addition, a follower forces assumption combined with a simplified stall model are assumed, in which the lift-curve slope is interpolated based on the experimental data available in the literature. Very good correlation between experimental and predicted aeroelastic responses has been obtained for a highly elongated plate-like wing structure with a ballast at the free end.

1 INTRODUCTION

In recent years, considerable efforts in the aeronautical industry has been dedicated towards the increase of the performance and the structural efficiency of the aircraft, still reducing its weight. The application of slender structures and new materials is one of the main strategies to achieve these requirements, which results in aircraft with higher aspect ratio and hence in structures with increased flexibility. Aircraft with high levels of flexibility are characterized by having low-frequency elastic modes, that may interact themselves in an unstable manner [1]. This makes it necessary to analyze the nonlinear aeroelasticity of the structure in order to better predict its true behavior. Therefore, this work focuses on the study of the nonlinear aeroelastic behavior of flexible structures applied to aircraft.

Several works have been published in the field of aeroelastic stability of flexible structures. Felippa [2] discusses theoretical aspects of a geometrically nonlinear finite element model applied to the Timoshenko's beam kinematics with linear interpolations and based on the total Lagrangian formulation. Drela [3] models a complete flexible aircraft as an assemblage of joined nonlinear beams with a co-rotational formulation. Also using the co-rotational approach Patil, Hodges, and Cesnik [4, 5] have studied the aeroelasticity and flight dynamics of HALE

aircraft. Siqueira and Coda [6] extended a total Lagrangian formulation developed for dynamic nonlinear analysis enclosing structural energy dissipation and sliding connections.

Differently from the most disseminated formulations (co-rotational and updated Lagrangian) found in the literature for dynamical analysis of geometrically nonlinear models, a finite element model for large displacements but small strains is presented herein. The apparatus analyzed in this work is a high-aspect-ratio wing with a ballast located at the tip. The finite element formulation is based on the total Lagrangian formulation, i.e., the quantities of a deformed configuration are calculated with respect to the initial configuration.

The nonlinear modeling is applied only for the bending motion since the torsion displacements are assumed linear and uncoupled to the bending displacements. The follower aerodynamic forces are computed using a 2D strip theory in the time domain with the Jones approximation for Wagner's function. In addition, a stall model is employed by admitting that the lift-curve slope for each strip is interpolated in each time step based on the aerodynamic experimental data for plate-like wing aerostructures available in the literature. The Newmark's method along with the Newton-Raphson method are used to solve the set of nonlinear dynamic equations.

2 STRUCTURAL MODEL

A rectangular thin plate is analyzed here in order to emulate the effects of an elongated flexible wing. For this, the plate is assumed to have 350 mm long, 40 mm wide, 0.81 mm thick, and made of aluminum, as shown in Fig. 1. The wing has a ballast fixed at its tip, emulating the effects of a concentrated mass. The ballast is a slender body which is allowed to be moved towards the leading or trailing edges to verify the effects of different inertia couplings on the aeroelastic stability of the wing.

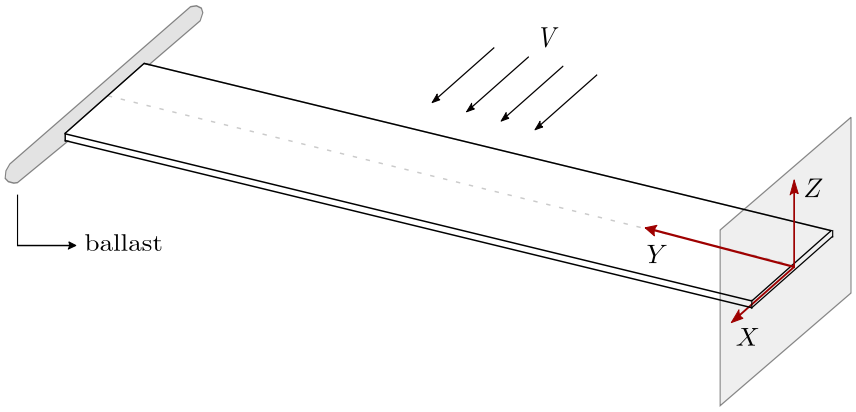

Figure 1: Plate-like wing with a ballast at the tip.

Several solid mechanics based theories are currently available in the literature for modeling the structural behaviour of beam-like structures. One of the simplest and most popular beam theory found in the literature is that described by Timoshenko, and discussed in many references, such as [7–10].

2.1 Timoshenko's beam kinematics

Based on the kinematics assumptions of a Timoshenko's beam, the exact reference-to-current bending mapping is formulated in a nonlinear sense, once large displacements and rotations are assumed. Consider then a generic material particle located at $P_0(X, Y, Z)$ in the initial configuration $\mathcal{C}_0$, which moves to $p(x, y, z)$ in the current configuration $\mathcal{C}$ due to the deformation of the beam, as can be seen in Fig. 2.

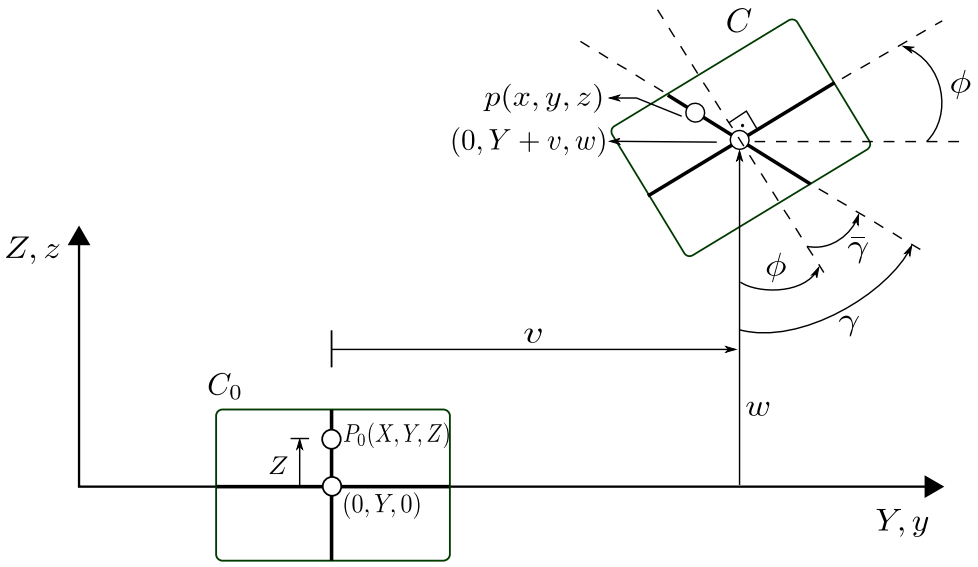

Figure 2: Kinematics of a Timoshenko's beam.

The point P_0 is referred to the local coordinate system XYZ in the initial configuration, whereas p is referred to the coordinate system xyz in the current configuration. A Total Lagrangian formulation is employed in this work to derive the beam kinematics; hence, the initial configuration $\mathcal{C}_0$ is taken as the reference frame for all physical quantities.

The following relations between the coordinates in each configuration are obtained assuming that the cross-sections are infinitely rigid and remains plane upon deformation, but not necessarily normal to the longitudinal axis after deformation ($\mathcal{C}_0 \rightarrow \mathcal{C}$) as

$$\left\{ \begin{array}{rcl} x &=& X \\ y &=& Y + v - Z\sin\gamma \\ z &=& w + Z\cos\gamma \end{array} \right. \tag{1}$$

where v, w and u ($u = 0$ for deformations in the plane YZ) are the displacements of the projection of $P_0(X, Y, Z)$ on the neutral axis in the XYZ reference system, and γ is the rotation of the cross-section.

The deformation gradient $\mathbf{F}$, related to the kinematics relations expressed in Eq. 1, is written in a polar decomposition form, which is convenient for the small strain assumption, as

$$\begin{aligned} \mathbf{F} &= \mathbf{R}(\gamma)\,\mathbf{U} \\ &= \underbrace{\begin{bmatrix} 1 & 0 & 0 \\ 0 & \cos\gamma & -\sin\gamma \\ 0 & \sin\gamma & \cos\gamma \end{bmatrix}}_{\text{rotation portion}} \underbrace{\begin{bmatrix} 1 & 0 & 0 \\ 0 & (1+v')\cos\gamma + w'\sin\gamma - Z\gamma' & 0 \\ 0 & -(1+v')\sin\gamma + w'\cos\gamma & 1 \end{bmatrix}}_{\text{stretch portion}} \end{aligned} \tag{2}$$

where $\mathbf{U}$ is the stretching matrix, and $\mathbf{R}$ is the rigid body rotation matrix.

In order to be consistent with the small strain assumption, it is convenient write the Green's tensor neglecting the rigid body rotation. Premultiplying both sides in Eq. 2 by $\mathbf{R}(-\gamma)$ leads to

the modified deformation gradient $\bar{\mathbf{F}} = \mathbf{U} = \bar{\mathbf{D}} - \mathbf{I}$, as

$$\begin{aligned} \bar{\mathbf{F}} &= \mathbf{R}(-\gamma)\mathbf{F} = \mathbf{U} \\ &= \begin{bmatrix} 1 & 0 & 0 \\ 0 & (1+v')\cos\gamma + w'\sin\gamma - Z\gamma' & 0 \\ 0 & -(1+v')\sin\gamma + w'\cos\gamma & 1 \end{bmatrix} \end{aligned} \tag{3}$$

The Green strain tensor can then be written in terms of the modified deformation gradient as

$$\mathbf{E_G} = \frac{1}{2}\left(\bar{\mathbf{F}}^T\bar{\mathbf{F}} - \mathbf{I}\right) = \frac{1}{2}\left(\bar{\mathbf{D}} + \bar{\mathbf{D}}^T\right) + \frac{1}{2}\bar{\mathbf{D}}^T\bar{\mathbf{D}} \tag{4}$$

The term $\bar{\mathbf{D}}^T\bar{\mathbf{D}}$ can now be neglected under the small-strains assumption, to find the following nonzero terms of the linear Green strain tensor

$$\begin{aligned} \epsilon_{yy} &= (1+v')\cos\gamma + w'\sin\gamma - 1 - Z\gamma' \\ &= e_0 - Z\kappa \end{aligned} \tag{5}$$

$$\bar{\gamma}_{yz} = -(v'+1)\sin\gamma + w'\cos\gamma \tag{6}$$

where e_0 is the membrane strain, κ is the curvature, and $\bar{\gamma}_{yz}$ is the shear strain.

In order to complete the aeroelastic formulation, torsion effects must be included in the formulation. The torsion is assumed linear and uncoupled from the bending motion; in addition, the Saint-Venant theory is applied to compute the torsion effects where the relationship between torsional moment $\bar{T}$ and shear strains are given as follows,

$$\bar{T} = GJ\bar{\gamma}_{xz} = GJ\theta' \tag{7}$$

where J is the torsional constant, and the product GJ is known as torsional rigidity.

The strain-displacement relationship can be written in a vector form as follows,

$$\begin{Bmatrix} e_0 \\ \kappa \\ \bar{\gamma}_{yz} \\ \bar{\gamma}_{xz} \end{Bmatrix} = \begin{Bmatrix} (1+v')\cos\gamma + w'\sin\gamma - 1 \\ \gamma' \\ -(v'+1)\sin\gamma + w'\cos\gamma \\ \theta' \end{Bmatrix} \tag{8}$$

2.2 Internal virtual work

Assuming a homogeneous and isotropic beam with length L, cross-section area A, and neglecting the pre-stress effects, the internal virtual strain energy, which is composed of the energies associated with the bending and torsion deformations, can be expressed as

$$\delta V_i = EA\int_0^L \left(H_{N1}\delta v' + H_{N2}\delta w' + H_{N3}\delta\gamma\right) dY + EI_x\int_0^L H_{M1}\delta\gamma'\, dY$$

$$+ \quad KGA \int_0^L \left(H_{Q1}\delta v' + H_{Q2}\delta w' + H_{Q3}\delta\gamma\right) dY + GJ \int_0^L H_{T1}\delta\theta'\, dY \tag{9}$$

where δ is the variational operator, I_x is the moment of inertia around X, K is the Timoshenko shear correction factor, and

$$\begin{aligned}
H_{N1} &= [w' \sin\gamma + (1+v')\cos\gamma - 1]\cos\gamma \\
H_{N2} &= [w' \sin\gamma + (1+v')\cos\gamma - 1]\sin\gamma \\
H_{N3} &= [w' \sin\gamma + (1+v')\cos\gamma - 1]\,[w'\cos\gamma - (1+v')\sin\gamma] \\
H_{M1} &= \gamma' \\
H_{Q1} &= [-w'\cos\gamma + (1+v')\sin\gamma - 1]\sin\gamma \\
H_{Q2} &= [w'\cos\gamma - (1+v')\sin\gamma - 1]\cos\gamma \\
H_{Q3} &= [-w'\cos\gamma + (1+v')\sin\gamma]\,[w'\sin\gamma + (1+v')\cos\gamma] \\
H_{T1} &= \theta'
\end{aligned} \tag{10}$$

are nonlinear expressions of the real displacements (with the exception of H_{T1} and H_{M1}, which are linear terms), i. e., they do not depend on any virtual displacement.

2.3 Virtual work due to inertias

A similar approach is employed to derive the inertial virtual work expression. It composed by three parts, the inertia provided by the bending and twisting motions of the beam, and the inertia of the translation and rotation motions of the ballast, resulting in the following expression of the total kinetic energy

$$\begin{aligned}
\delta T &= \rho A \int_0^L \dot{v}\,\delta\dot{v}\, dY + \rho A \int_0^L \dot{w}\,\delta\dot{w}\, dY + \rho I_x \int_0^L \dot{\gamma}\,\delta\dot{\gamma}\, dY + \rho I_y \int_0^L \dot{\theta}\,\delta\dot{\theta}\, dY \\
&+ m_{\text{blt}}\left[\dot{v}(L)\,\delta\dot{v}(L) + \dot{w}(L)\,\delta\dot{w}(L)\right] + m_{\text{blt}}\Delta d_{blt}\left[\dot{w}(L)\,\delta\dot{\theta}(L) + \dot{\theta}(L)\,\delta\dot{w}(L)\right] \\
&+ \left(I_{y_{\text{blt}}} + m_{\text{blt}}\Delta d_{blt}^2\right)\dot{\theta}(L)\,\delta\dot{\theta}(L)
\end{aligned} \tag{11}$$

where I_y is the moment of inertia around Y, ρ is the material density, and m_{blt} and $I_{y_{\text{blt}}}$ are the mass and the moment of inertia around Y of the ballast, respectively. Furthermore, Δd_{blt} is the distance between the center of mass of the beam and the center of mass of the ballast, measured along the plate-like wing chordwise direction (X-direction). The term $m_{\text{blt}}\Delta d_{blt}^2$ denotes an additional second moment of inertia as a result of the Steiner's theorem (or parallel axis theorem), whereas $m_{\text{blt}}\Delta d_{blt}$ denotes the first moment of inertia. The latter couples the transversal translation and the torsion motions.

3 AERODYNAMIC MODEL

Aerodynamic models based on 2D linear potential theory are suitable for aeroelastic analysis of highly elongated wings under subsonic flow, where flow compressibilty and viscosity effects can be negligible, as found in [11, 12].

Wagner's theory [13] is employed to represent the unsteady formulation of the aerodynamic loads on a thin plate-like wing undergoing an arbitrary motion. A time-domain description for the aerodynamics is obtained by applying the Jones' approximation for Wagner's indicial

function [14]. Furthermore, for accounting the aerodynamic effects of the stall and/or finite span, the Yates' modified strip theory method [15] is applied, as reported in [16]. Effects of large displacements are also computed through the follower forces assumption.

3.1 Modified strip theory method

The strip theory is one of the most simple strategies employed together with finite element beam model for modeling the spanwise aerodynamic load distribution of a lifting surface, providing a good aerodynamic approximation for high aspect ratio wings. The strip theory assumes the wing to be discretized in spanwise strips of finite width, where each strip is treated as an individual airfoil, with no interaction between neighboring strips.

It is also assumed that the lift and moment on each strip of the wing are proportional to the local pitch and plunge, which are in this work represented by the vertical displacement w and the torsion angle θ, respectively. These aerodynamic forces are defined along the mid-chord of the wing and act on sections perpendicular to the mid-chord line [17].

Then, by using the principle of virtual work, the effects of the non-conservative aerodynamic loads computed via the modified strip theory acting on the wing can be expressed in a summation form as

$$\delta W^{aer} = \sum_{j=1}^{n_j} \left(l_j^{aer} \delta w_j + m_j^{ea} \delta \theta_j \right) \Delta y_j \tag{12}$$

where l_j^{aer} and m_j^{ea} are the lift force and the pitching moment per unit span regarding the j-th strip, and n_j is the total number of strips. For convenience, we admit the number of strips equal to the number of elements, and the center of each strip coincident with the nodes. These assumptions are taken in order to avoid any interpolation from the structural degrees of freedom to the aerodynamic ones.

Figure 3 shows in details the schematic of the j-th strip at the position y_j in the spanwise direction, with width Δy_j, chord length c_j (or the related semi-chord b_j), aerodynamic centre position a_{cj} (in semi-chords), and the elastic axis position a_j (in semi-chords). Note that, the aerodynamic centre position, the chord length, and the elastic axis are assumed to be constant along the span ($a_{cj} = -0.5$, $c_j = 2b$, and $a_j = 0$), since a rectangular (untapered) and uniform wing has been modeled here.

Considering a lifting surface flying at velocity V, the aerodynamic forces acting on each strip can be expressed as [16],

$$l_j^{aer}(t) = \pi \rho b_j^2 \left(-\ddot{w}_j + V\dot{\theta}_j - b_j a_j \ddot{\theta}_j \right) + C_{l\alpha j} \rho V b_j \left[Q_{3/4j}(t) + \lambda_{1j}(t) + \lambda_{2j}(t) \right] \tag{13}$$

$$\begin{aligned} m_j^{ea}(t) = {} & \pi \rho b_j^2 \left[-V\dot{w}_j - b_j a_j \ddot{w}_j + V^2 \theta_j - b_j^2 \left(\frac{1}{8} + a_j^2 \right) \ddot{\theta}_j \right] \\ & - \pi \rho V b_j^2 \left[Q_{3/4j}(t) \right] + b_j \left(a_j - a_{cj} \right) l_j^{(c)}(t) \end{aligned} \tag{14}$$

where λ_{1j} and λ_{2j} represent the lag for the local lift to respond to an arbitrary change in the downwash, and they are determined by solving the two following first order differential equations for each strip

$$\dot{\lambda}_{1j}(t) = -0.0455 \frac{V}{b_j} \lambda_{1j}(t) - 0.165 \dot{Q}_{\frac{3}{4}j}(t)$$

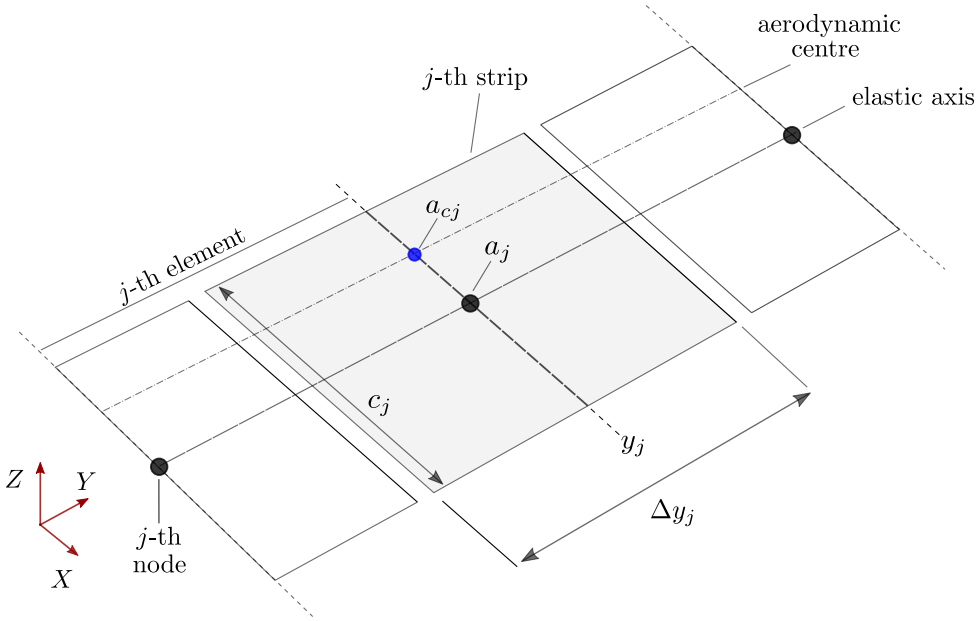

Figure 3: Strips schematic assumed here.

$$\dot{\lambda}_{2j}(t) \quad = \quad -0.3000\frac{V}{b_j}\lambda_{2j}(t) - 0.335\dot{Q}_{\frac{3}{4}j}(t) \tag{15}$$

Moreover,

$$Q_{3/4j} \quad = \quad V\theta_j - \dot{w}_j + b_j\left(\frac{C_{l\alpha j}}{2\pi} + a_{cj} - a_j\right)\dot{\theta}_j \tag{16}$$

is the downwash related to the j-th strip at three-quarter chord position.

In order to compute the effects of large deflections, a follower forces assumption is incorporated into the aerodynamic model. Nevertheless, the pressure distribution is assumed to vary linearly owing to the nonlinear structural deformation. Instead, the aerodynamic loads are just rotated from their local strip frames to the global frame. Both bending and twisting rotations are admitted to modify the local lift in each strip. This effect is taken into account by a transformation matrix as

$$\mathbf{f^{aer}}_j = \mathbf{r^{gl}}_j \left\{ \begin{array}{c} 0 \\ l_j^{aer} \\ 0 \\ m_j^{ea} \end{array} \right\} \tag{17}$$

where $\mathbf{r^{gl}}_j$ is the rotation matrix from the local strip frame to the global frame.

A simple stall model is also enclosed in the aerodynamic model to complete the nonlinear aeroelastic representation of flying wings. In addition, this phenomenon was observed in previous works involving this kind of aeroelastic apparatus, such as [18, 19]. The stall effects are accounted through a static distribution of lift coefficient C_l as a function of the angle of attack. The values of C_l employed here were experimentally obtained by Pelletier and Mueller [20], in a study of thin flat plates on low Reynolds number.

At this point, the aerodynamic loads accounting for the stall and follower forces models can be expressed in a matrix form as

$$\mathbf{f^{aer}}_j = \mathbf{r^{gl}}_j \left\{ \mathbf{a_1}_j \left\{ \begin{array}{c} \ddot{v}_j \\ \ddot{w}_j \\ \ddot{\gamma}_j \\ \ddot{\theta}_j \end{array} \right\} + \mathbf{a_2}_j \left\{ \begin{array}{c} \dot{v}_j \\ \dot{w}_j \\ \dot{\gamma}_j \\ \dot{\theta}_j \end{array} \right\} + \mathbf{a_3}_j \left\{ \begin{array}{c} v_j \\ w_j \\ \gamma_j \\ \theta_j \end{array} \right\} + \mathbf{a_4}_j \left\{ \begin{array}{c} \lambda_{1j} \\ \lambda_{2j} \end{array} \right\} \right\} \Delta y_j \tag{18}$$

with the following associated lag states dynamics

$$\left\{ \begin{array}{c} \dot{\lambda}_{1j} \\ \dot{\lambda}_{2j} \end{array} \right\} = \mathbf{b_1}_j \left\{ \begin{array}{c} \ddot{v}_j \\ \ddot{w}_j \\ \ddot{\gamma}_j \\ \ddot{\theta}_j \end{array} \right\} + \mathbf{b_2}_j \left\{ \begin{array}{c} \dot{v}_j \\ \dot{w}_j \\ \dot{\gamma}_j \\ \dot{\theta}_j \end{array} \right\} + \mathbf{b_3}_j \left\{ \begin{array}{c} v_j \\ w_j \\ \gamma_j \\ \theta_j \end{array} \right\} + \mathbf{b_4}_j \left\{ \begin{array}{c} \lambda_{1j} \\ \lambda_{2j} \end{array} \right\} \tag{19}$$

and where $\mathbf{a_{(1\ldots4)j}}_j$ and $\mathbf{b_{(1\ldots4)}}_j$ are the local aerodynamic matrices.

4 AEROELASTIC PROBLEM FORMULATION

The dynamics of a thin clamped-free plate subjected to a subsonic flow with airspeed V along the chord-wise direction X is imposed on the wing, just as depicted in Fig. 1. The governing equations of motion can be derived from the energy-based Hamilton's Principle, which is mathematically stated as

$$\int_{t_1}^{t_2} \delta \left(T - V_i \right) dt + \int_{t_1}^{t_2} \delta W^{ext} \, dt = 0 \tag{20}$$

Considering a two-node, prismatic, straight, and 2D Timoshenko beam element moving in the plane YZ, with 8 degrees of freedom, 4 per node. There are four displacement fields to be interpolated, i.e. v, w, γ, and θ. In order to preserve the field consistency (continuity condition), the displacements are independent and expressed as linear functions of the node displacements, also known as Lagrange interpolation functions.

Collecting the degrees of freedom of an element in a vector, we can define the element displacements vector $\mathbf{d}$,

$$\mathbf{d} = \left\{ \begin{array}{cccccccc} v_1, & w_1, & \gamma_1, & \theta_1, & v_2, & w_2, & \gamma_2, & \theta_2 \end{array} \right\}^T \tag{21}$$

Assuming that all components of $\delta\mathbf{d}$ are independent and arbitrary, and using the usual global matrix assembling process involving the element matrices of a beam discretized in n_e elements, the Hamilton's Principle can then be rewritten in a more convenient and usual form, as

$$\mathbf{M}\ddot{\tilde{\mathbf{d}}} + \mathbf{F_{int}}(\tilde{\mathbf{d}}) = \tilde{\mathbf{F}}^{\mathbf{aer}} \tag{22}$$

where $\tilde{\mathbf{d}}$, $\mathbf{M}$, $\mathbf{F}_{\text{int}}$,and $\tilde{\mathbf{F}}^{\mathbf{aer}}$ are the global displacements vector, the nonlinear internal forces vector, the aerodynamic forces vector, and the global mass matrix, respectively.

Assuming the modified strip theory, described in Section 3 to compute the aerodynamic loads, and incorporating the follower forces and stall assumptions, the global equations of motion lead to

$$\mathbf{M}\ddot{\tilde{\mathbf{d}}} + \mathbf{F}_{\text{int}}(\tilde{\mathbf{d}}) = \mathbf{R^{gl}}(\tilde{\mathbf{d}}) \Big\{ \mathbf{A_1}\ddot{\tilde{\mathbf{d}}} + \mathbf{A_2}(\tilde{\mathbf{d}})\dot{\tilde{\mathbf{d}}} + \mathbf{A_3}(\tilde{\mathbf{d}})\tilde{\mathbf{d}} + \mathbf{A_4}(\tilde{\mathbf{d}})\boldsymbol{\lambda} \Big\} \tag{23}$$

along with the following global associated lag states dynamics,

$$\dot{\boldsymbol{\lambda}} = \mathbf{B_1}(\tilde{\mathbf{d}})\ddot{\tilde{\mathbf{d}}} + \mathbf{B_2}\dot{\tilde{\mathbf{d}}} + \mathbf{B_3}\tilde{\mathbf{d}} + \mathbf{B_4}\boldsymbol{\lambda} \tag{24}$$

where $\mathbf{A_{(1\ldots4)}}$ and $\mathbf{B_{(1\ldots4)}}$ are the global aerodynamic matrices, $\mathbf{R^{gl}}$ is the global rotation matrix regarding the follower forces assumption, and $\boldsymbol{\lambda}$ is the global lag states vector.

Finally, by using Eqs. 23 and 24, the extended nonlinear second order equations of motion of the aeroelastic system can be written as

$$\begin{aligned}
&\begin{bmatrix} \left[\mathbf{M} - \mathbf{R^{gl}}(\tilde{\mathbf{d}})\mathbf{A_1}\right] & \mathbf{0} \\ -\mathbf{B_1}(\tilde{\mathbf{d}}) & \mathbf{0} \end{bmatrix} \begin{Bmatrix} \ddot{\tilde{\mathbf{d}}} \\ \ddot{\boldsymbol{\lambda}} \end{Bmatrix} + \begin{bmatrix} -\mathbf{R^{gl}}(\tilde{\mathbf{d}})\mathbf{A_2}(\tilde{\mathbf{d}}) & \mathbf{0} \\ -\mathbf{B_2} & \mathbf{I} \end{bmatrix} \begin{Bmatrix} \dot{\tilde{\mathbf{d}}} \\ \dot{\boldsymbol{\lambda}} \end{Bmatrix} \\
&+ \begin{bmatrix} -\mathbf{R^{gl}}(\tilde{\mathbf{d}})\mathbf{A_3}(\tilde{\mathbf{d}}) & -\mathbf{R^{gl}}(\tilde{\mathbf{d}})\mathbf{A_4}(\tilde{\mathbf{d}}) \\ -\mathbf{B_3} & -\mathbf{B_4} \end{bmatrix} \begin{Bmatrix} \tilde{\mathbf{d}} \\ \boldsymbol{\lambda} \end{Bmatrix} + \begin{Bmatrix} \mathbf{F_{int}}(\tilde{\mathbf{d}}) \\ \mathbf{0} \end{Bmatrix} = \mathbf{0}
\end{aligned} \tag{25}$$

or just,

$$\overline{\mathbf{M}}(\mathbf{q})\ddot{\mathbf{q}} + \overline{\mathbf{C}}(\mathbf{q})\dot{\mathbf{q}} + \overline{\mathbf{K}}(\mathbf{q})\mathbf{q} + \overline{\mathbf{F}}_{\mathbf{int}}(\mathbf{q}) = \mathbf{0} \tag{26}$$

where $\overline{\mathbf{M}}$, $\overline{\mathbf{C}}$, $\overline{\mathbf{K}}$ are the extended nonlinear mass, damping, and stiffness matrices, respectively. In addition, $\overline{\mathbf{F}}_{\mathbf{int}}$ is the extended nonlinear internal forces vector, and $\mathbf{q}$ is the extended displacements vector. These quantities are given by

$$\begin{aligned}
\overline{\mathbf{M}} &= \begin{bmatrix} \left[\mathbf{M} - \mathbf{R^{gl}}(\tilde{\mathbf{d}})\mathbf{A_1}\right] & \mathbf{0} \\ -\mathbf{B_1}(\tilde{\mathbf{d}}) & \mathbf{0} \end{bmatrix}; \quad \overline{\mathbf{K}} = \begin{bmatrix} -\mathbf{R^{gl}}(\tilde{\mathbf{d}})\mathbf{A_3}(\tilde{\mathbf{d}}) & -\mathbf{R^{gl}}(\tilde{\mathbf{d}})\mathbf{A_4}(\tilde{\mathbf{d}}) \\ -\mathbf{B_3} & -\mathbf{B_4} \end{bmatrix} \\
\overline{\mathbf{C}} &= \begin{bmatrix} -\mathbf{R^{gl}}(\tilde{\mathbf{d}})\mathbf{A_2}(\tilde{\mathbf{d}}) & \mathbf{0} \\ -\mathbf{B_2} & \mathbf{I} \end{bmatrix}; \qquad \mathbf{q} = \begin{Bmatrix} \tilde{\mathbf{d}} \\ \boldsymbol{\lambda} \end{Bmatrix}; \qquad \overline{\mathbf{F}}_{\mathbf{int}} = \begin{Bmatrix} \mathbf{F_{int}}(\tilde{\mathbf{d}}) \\ \mathbf{0} \end{Bmatrix}
\end{aligned} \tag{27}$$

The solution of the dynamic governing set of equations, Eq. 26 is achieved by using Newmark's method [21], which is a method based on a fixed time-step Δt. It is an implicit time integration method, i.e, the solution at time $i+1$ (as reference for the time $i\Delta t + \Delta t$) is determined by the equilibrium condition at time $i+1$. The Newton-Raphson method is then applied to iterate the displacements in each time step based on the dynamic tangent stiffness matrix.

5 NUMERICAL RESULTS

The nonlinear structural model adopted in this work was first compared against results from the literature to demonstrate the accuracy and efficiency of the proposed element, either in static or dynamic cases of beams under large bending deflections but small strain and undergoing concentrated loads.

Additionally aeroelastic stability analyses results for an isotropic and elongated plate-like wing with a ballast at the tip were compared to results from experimental tests and obtained using Nastran FE code. And finally, the numerical nonlinear dynamic response in terms of the amplitudes of the limit cycle oscillations were also compared with the experimental results obtained from wind tunnel aeroelastic tests.

5.1 Static analysis

The static equilibrium equations are obtained from Eq. 20neglecting inertial effects and assuming the external forces are not time-dependent, resulting then in the so-called Principle of Virtual Works as

$$\mathbf{\Psi}(\tilde{\mathbf{d}}) = \mathbf{f}_{\text{int}}(\tilde{\mathbf{d}}) - \mathbf{f}^{\mathbf{ext}} = \mathbf{0} \tag{28}$$

where $\mathbf{\Psi}$ is the nonlinear unbalanced forces vector.

A cantilever beam under an end moment, as shown in Fig. 4, is the most employed benchmark for inspecting the robustness of geometrically nonlinear beam models, since the analytical solution is readily available, as done in [22–24].

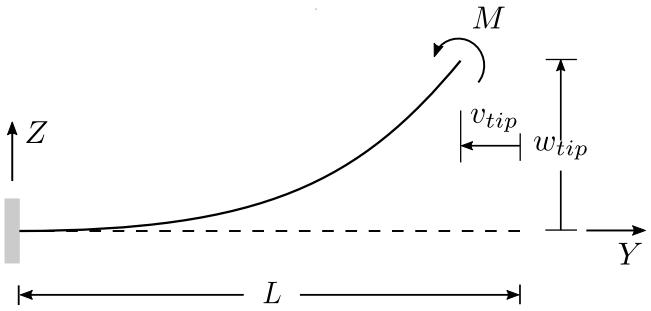

Figure 4: Cantilever beam with an end point moment.

The equilibrium responses are determined by taking successive load increments and applying the Newton-Raphson method to iterate the displacements and obtain the convergence for each load increment. The tolerance values assumed here were $\varepsilon_{\mathbf{g}} = 10^{-3}$ N and $\varepsilon_{\mathbf{q}} = 10^{-4}$ m, with a maximum number of 30 iterations in each load step. Besides that, an integration scheme with one-point Gauss quadrature scheme was used to properly alleviate the membrane and shear locking presented by this element.

A beam with length $L = 3.2$ m, cross-section area $A = 10^{-2}$ m^2, Young's modulus $E = 210$ GPa, shear modulus $G = 79$ GPa, and shear correction factor $K = 5/6$ was considered for this analysis. The beam is subjected to a moment $M = M^* L/2\pi EI$, with the normalized moment M^* varying from 0 up to 6. The values $ML/2\pi EI = n_l$ correspond to the analytical solution to accomplish n_l loops in the beam. Furthermore, the displacement components of the free end are now related to the finite element displacements by $v_{tip} = -v(L)$ and $w_{tip} = w(L)$.

The numerical results are compared with those computed analytically in Fig. 5, where a good agreement between numerically predicted and closed form solutions was found. For this, a refined mesh with 50 elements was employed; however, the model already presents good results with only 5 elements. Figure 6 still presents the beam deformations for some values of M^*.

5.2 Dynamic analysis

In order to also validate the dynamic response of the model and the time integration method, this section presents a case of a cantilever beam subjected to a triangular load and taking into account viscous damping effects. However, only velocity proportional damping is computed here, neglecting any other dissipative mechanisms. Figure 7 depicts the beam properties and the load history, given in SI units and presented in [25]. The integration of the dynamic equilibrium

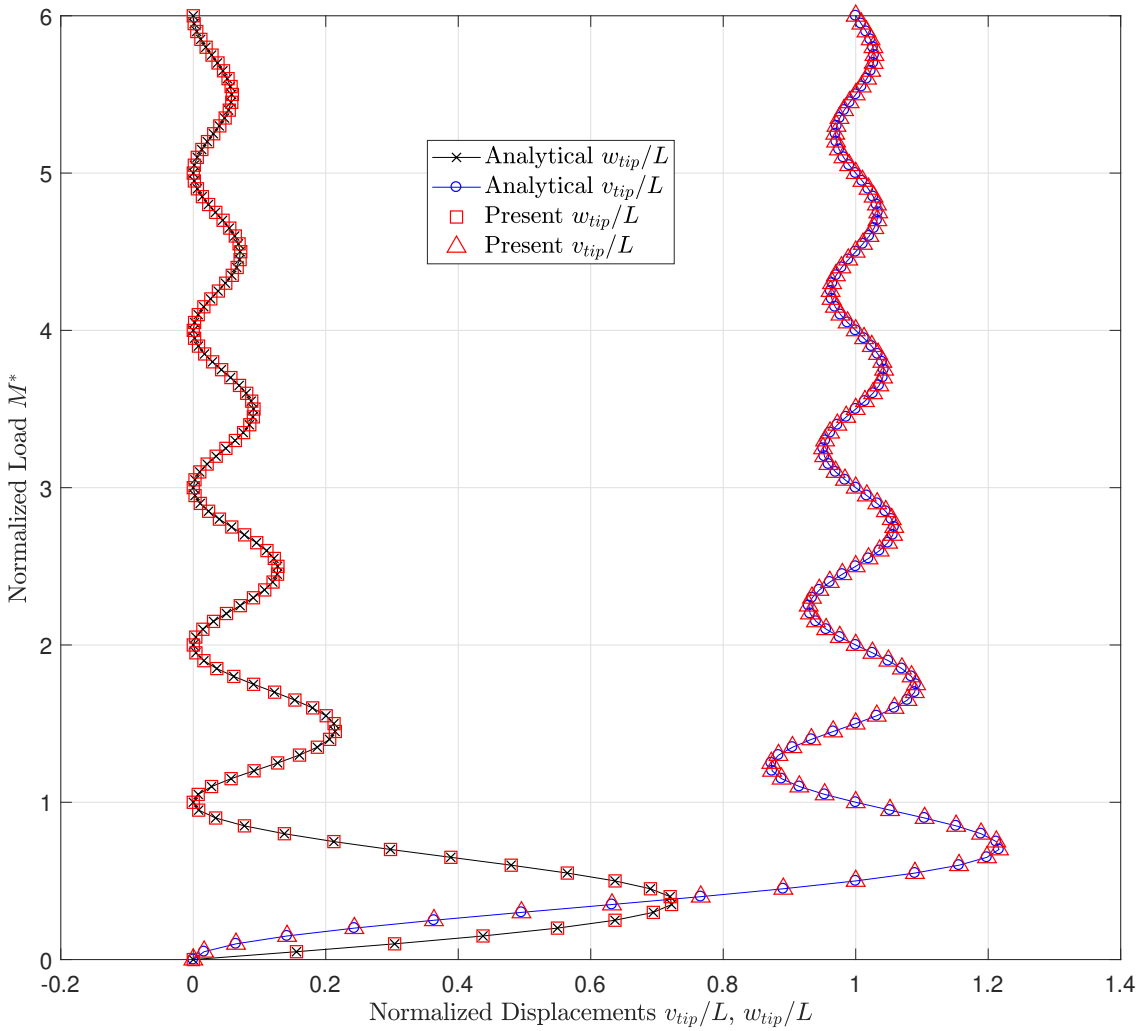

Figure 5: Load-deflection curves for a moment applied at the tip.

equation is performed in the time interval $t = [0, 100]$ s, and for this, a beam discretization with 10 elements is employed.

The obtained results are compared with the results reported by Simo [25] in Fig. 8. The results indicate good agreement between numerical predictions obtained using the proposed model and the Simo's solutions.

After the validation of the structural finite element model developed here, the aeroelastic model is further evaluated and the predicted aeroelastic responses obtained using the proposed model are compared with experimental and numerical results obtained using Nastran FE code.

5.3 Aeroelastic analysis

In a first moment, the aeroelastic stability analyzes of the rectangular thin wing shown in Fig. 9 were performed through the model linearization and the subsequent solution of the eigenvalue problem to obtain the flutter and divergence speeds based on the V-g diagram. The properties of the wing are summarized in Table 1. The present results were performed using 35 elements and they are compared with a strip theory model performed with a beam finite element model implemented in Nastran also with 35 elements. Furthermore, experimental results were also

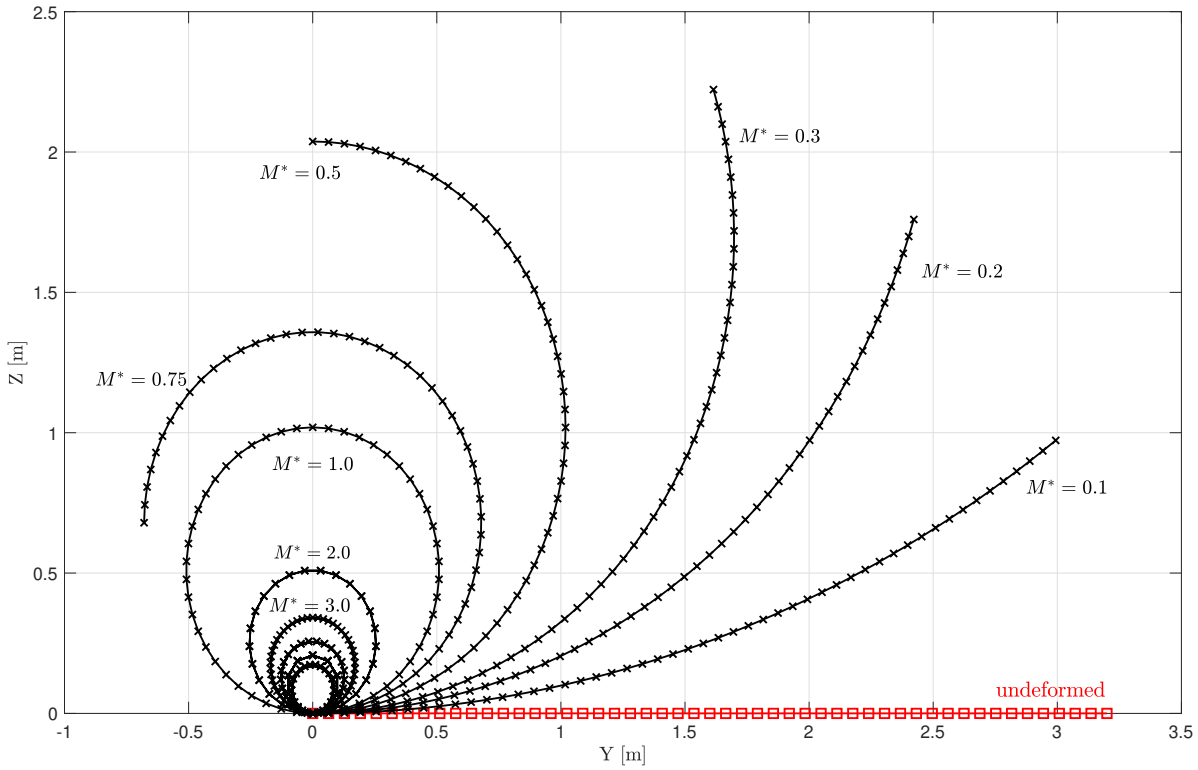

Figure 6: Beam deformation for progressive moment at the free end.

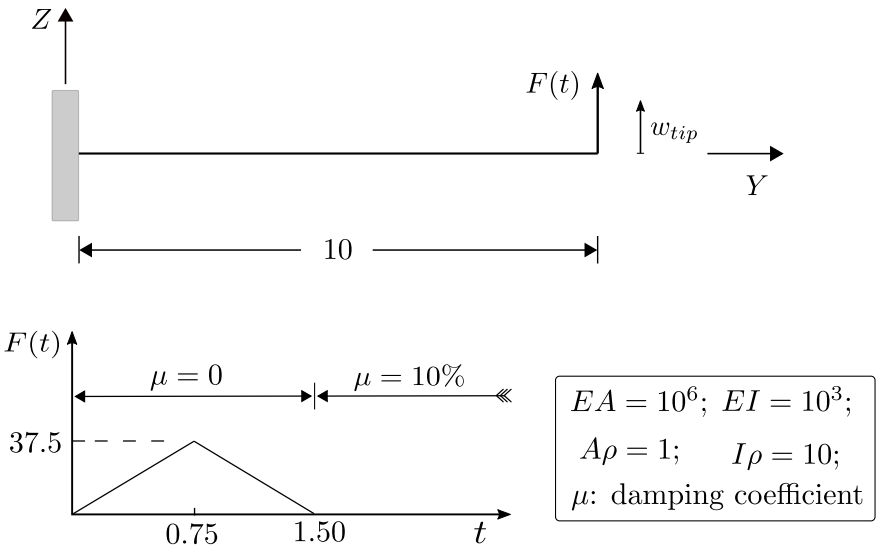

Figure 7: Cantilever beam geometry and load history.

used to validate the present results in terms of the aeroelastic stability analyzes.

Table 2 compares the flutter speeds obtained using the proposed model against those from Nastran and experiments, where a fairly good correlation between these results was found. For instance, the mean error between the experimental and results obtained using the proposed model is about 7%. Moreover, in all cases addressed in this work, the flutter phenomenon was achieved by the coupling between the first torsion and the second bending modes, the same as verified during the aeroelastic experiments.

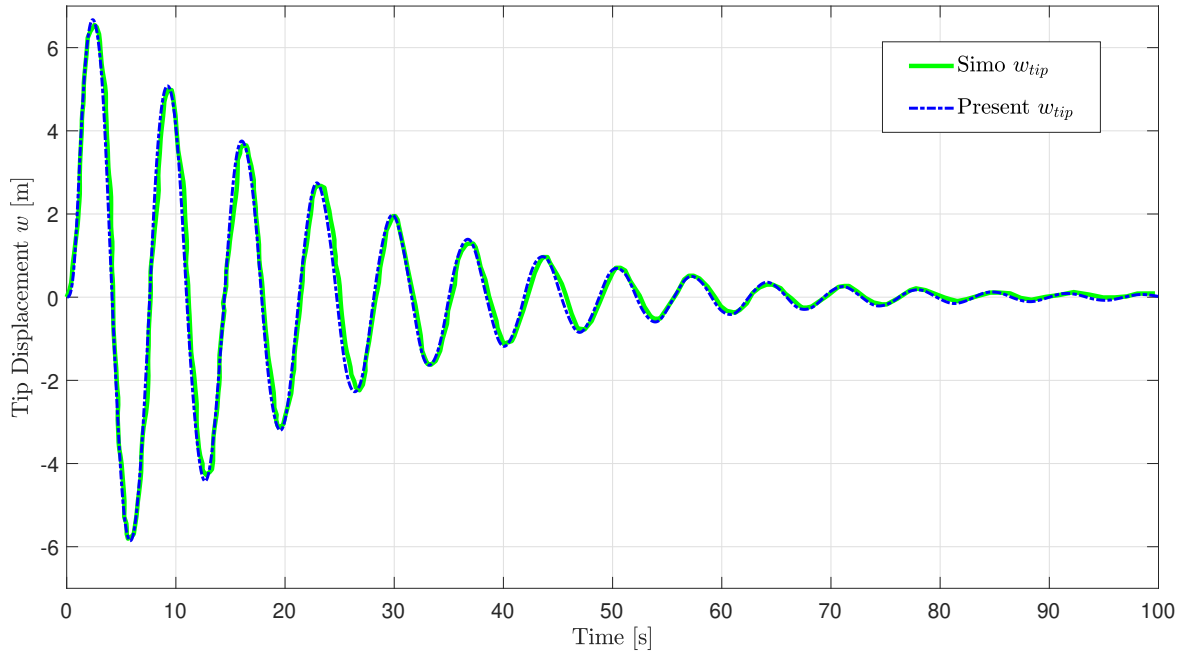

Figure 8: Tip displacement history of a damped beam.

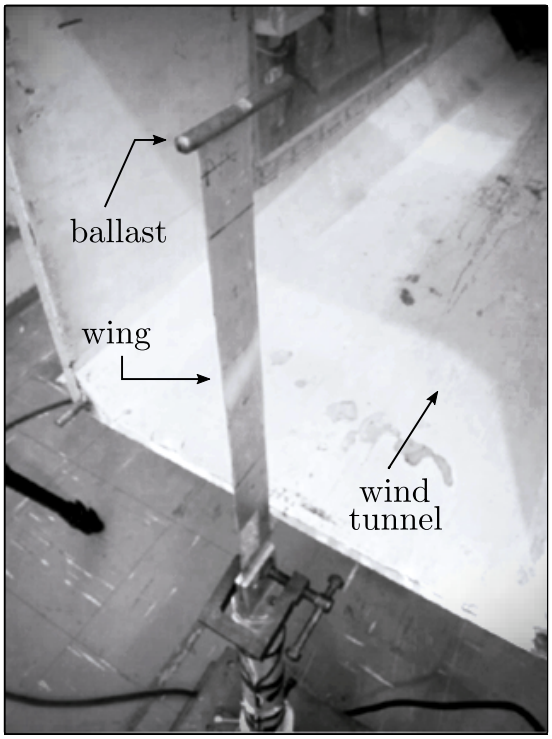

Figure 9: Wing at the wind tunnel during the experiments.

The numerical nonlinear dynamic response in terms of LCO amplitude is compared with the experimental results in Fig. 10. The vertical displacements w of the wing tip were measured by a laser vibrometer and compared with the present results for an airspeed of 11 m/s and a ballast position of -5 mm along the chord-wise direction. This comparison has shown a good agreement between the responses, with an error of about 9% in the transversal displacement and 12% in the torsion angle.

Table 1: Wing geometry, material and inertia properties.

Parameter	Value	Unit
Span, L	350	mm
Chord, c	40	mm
Thickness h	0.81	mm
Density, ρ	2780	kg/m^3
Young's modulus, E	73.1	GPa
Shear modulus, G	27.5	GPa
Ballast mass, m_{blt}	34.5	g
Ballast inertias, $I_{x_{blt}}$, $I_{y_{blt}}$	0.186	cm^4

Table 2: Flutter speed for different ballast positions.

Ballast Position	0 mm	-5 mm	-10 mm	-15 mm	no ballast
Nastran [m/s]	10.48	10.09	12.03	14.34	46.37
Experimental [m/s]	-	10.5	13.00	15.00	-
Present [m/s]	9.50	9.80	12.30	14.70	47.30

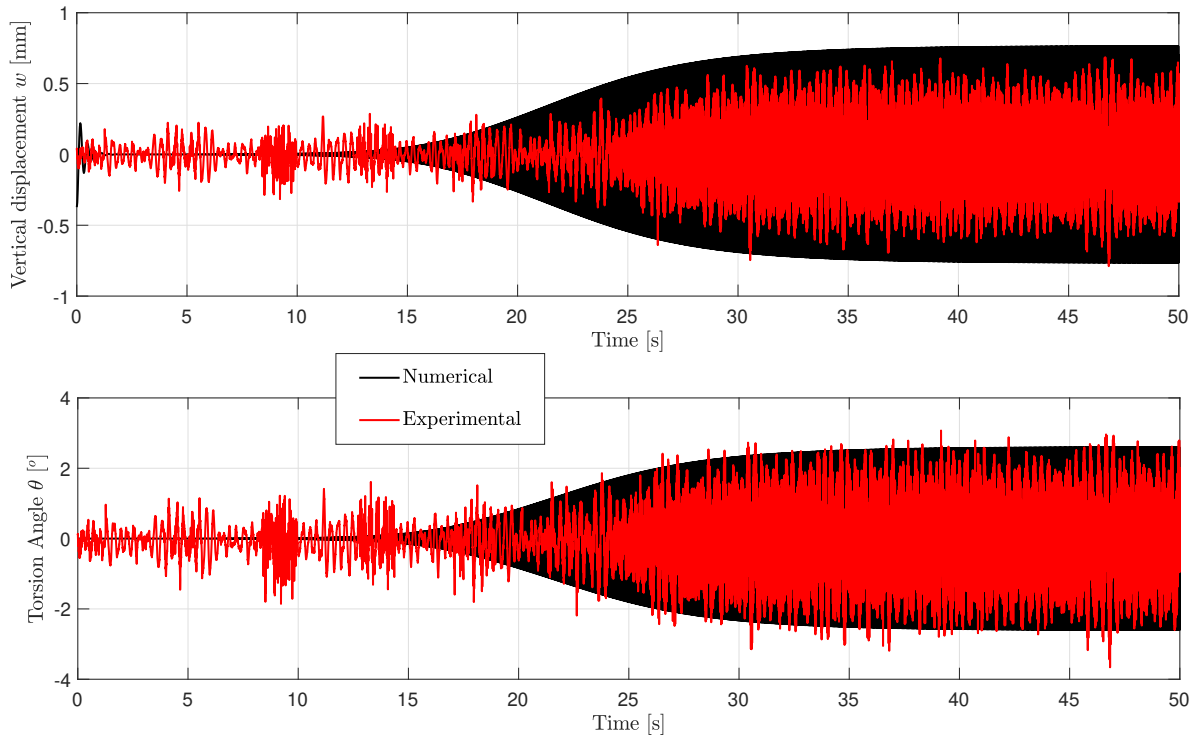

Figure 10: Comparison of the LCO amplitude between the present and experimental results for $V = 11$ m/s and $\Delta d_{blt} = -5$ mm.

Figure 11 compares the contribution of the nonlinearity regarding the large deflections with those related to the stall model in the LCO amplitude, where the stall presents a larger contribution than the geometric nonlinearity. Nevertheless, both nonlinearities together present a greater result when compared with those from experiments.

The phase plane regarding the numerical results presented in Fig. 10 is presented in Fig. 12,

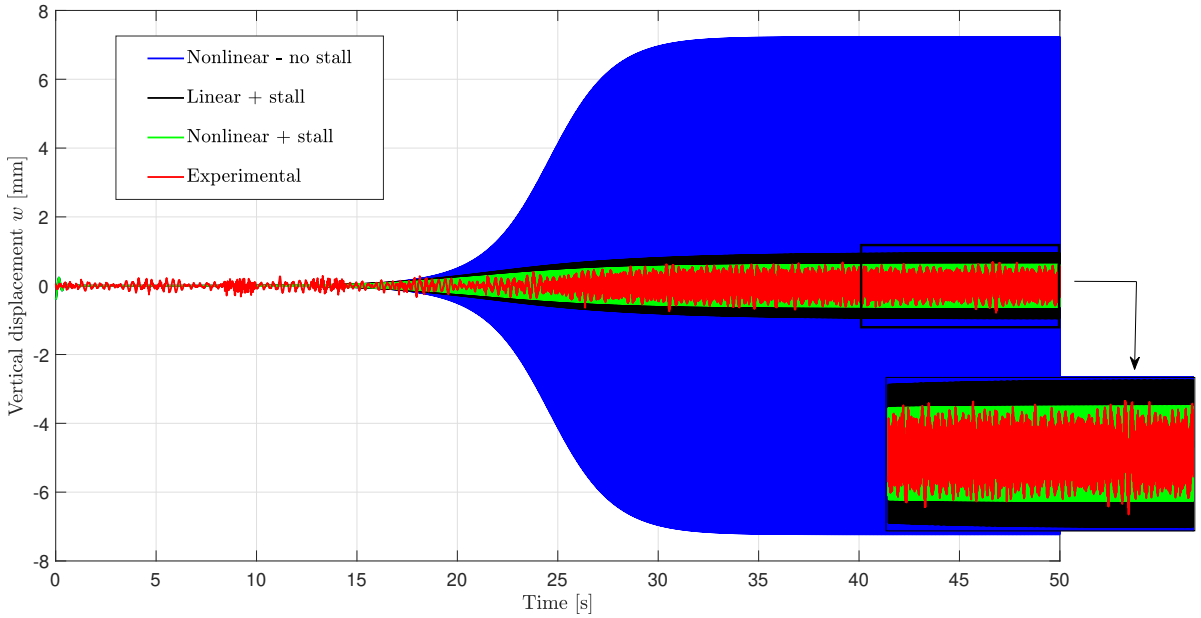

Figure 11: Comparison of stall and geometric nonlinearities contributions in the LCO amplitude.

where the transversal displacement of the wing tip and the respective velocity indicates a classic periodic limit cycle oscillation.

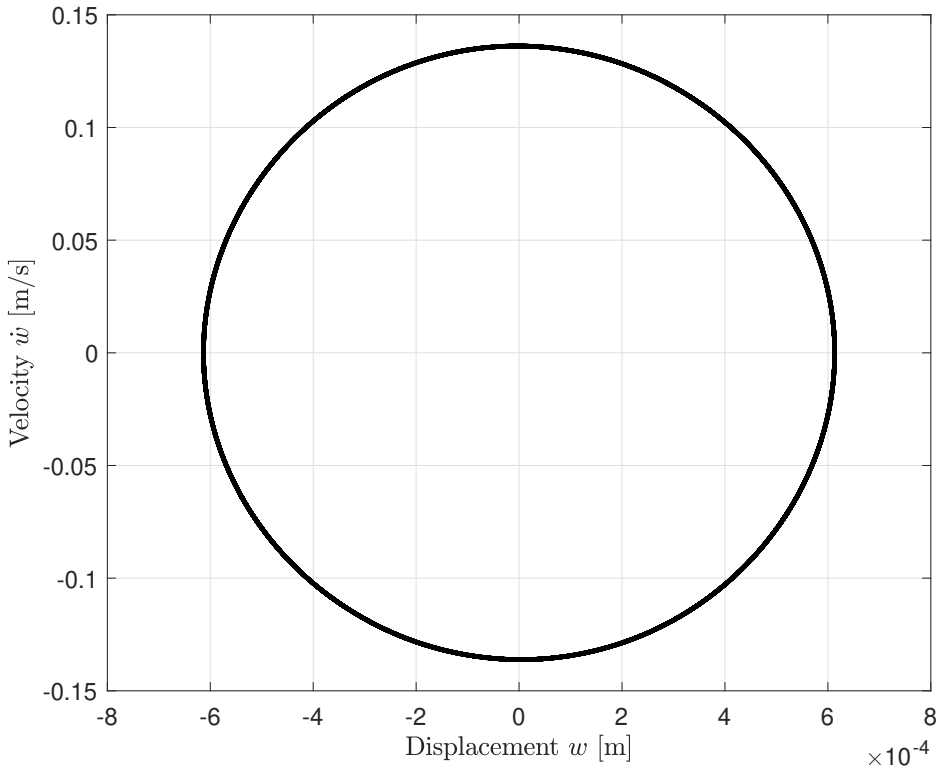

Figure 12: Phase plane related to the numerical result.

Figure 13 compares the measured and numerical LCO amplitudes considering both w and θ for different airspeeds. Note that as the airspeed increases the error between predicted and measured torsion angle also increases. This trend error is mainly due to assumptions initially

adopted regarding torsion modeling, which are limited to linear uniform torsion.

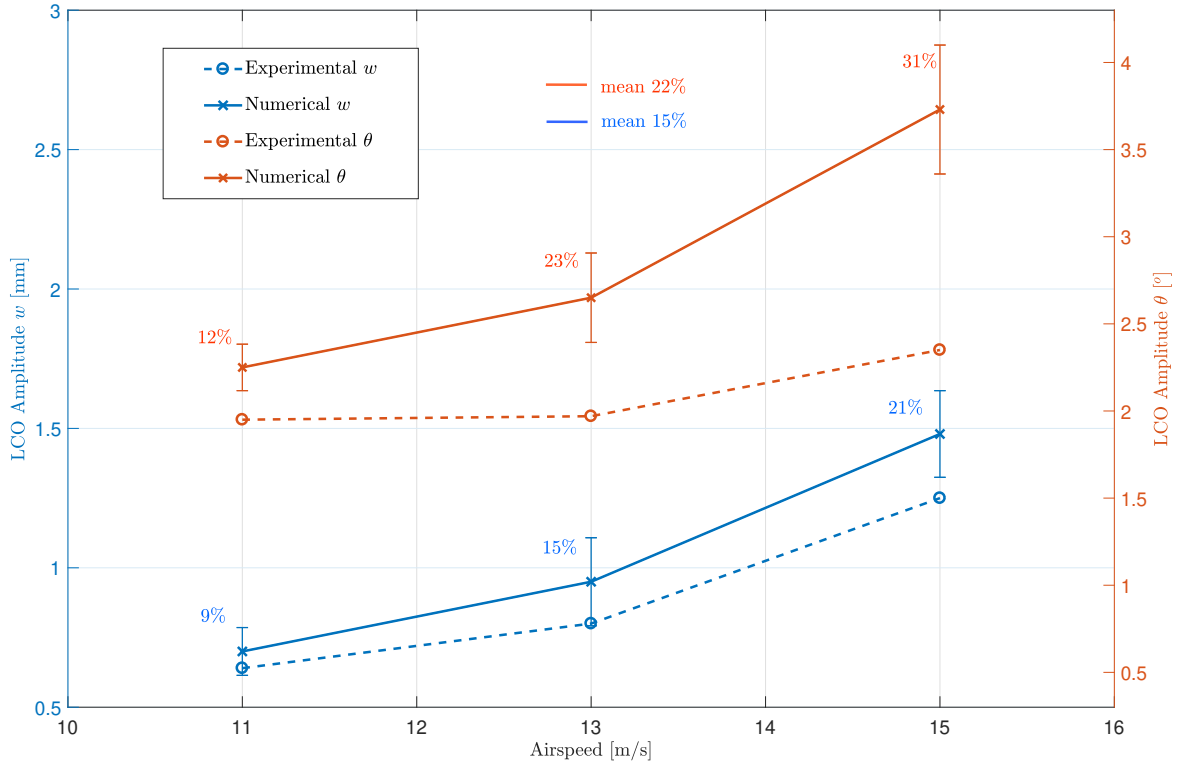

Figure 13: Results summary: Comparison between measured and predicted LCOs amplitudes for different airspeeds.

6 CONCLUSIONS

The current work presented a beam finite element model accounting for geometric and aerodynamic nonlinearities due to large deflections through the total Lagrangian kinematic description. High aspect-ratio wings manufactured in isotropic materials coupled to a time-domain strip theory aerodynamic model that accounts the stall and follower aerodynamic forces were implemented and analyzed here.

The proposed formulation is limited to small strains. This assumption makes the mathematical formulation of the governing equations more friendly, on the other hand, it is not suitable for some structural problems.

The possibility of using very high flexible wings to improve the aerodynamic efficiency in the aircraft opens new possibilities of unexpected behaviors related to instabilities of aeroelastic nature. As shown in this work, nonlinear beam models with low computational cost are able to represent the true aeroelastic behavior of high flexible wings, where the aeroelastic responses predicted by these models correlate fairly well with the experimental results.

Currently, aeroelastic optimization is an integral part of formal procedures for aircraft designers evaluate during many project phases. Then, this work moves toward one of the main research subjects addressed in the last years in the aeronautical and aerospace fields. More broadly, all of these proposed studies have the objective of making high flexible aircraft very efficient from the aeroelastic point of view.

7 ACKNOWLEDGMENTS

This work has been funded by Brazilian agencies Coordenação de Aperfeiçoamento de Pessoal de Nível Superior - CAPES, National Council for Scientific and Technological Development (CNPq), Process No. 301053/2016-2, Instituto de Pesquisas Tecnológicas do Estado de São Paulo S. A. - IPT, and by Fundação de Apoio ao Instituto de Pesquisas Tecnológicas do Estado de São Paulo - FIPT (grants Programa Novos Talentos).

8 REFERENCES

[1] Silva, G. C., Silvestre, F. J., Donadon, M. V., et al. (2018). Active and passive control for acceleration reduction of an aeroelastic typical wing section. *Journal of Vibration and Control*.

[2] Felippa, C. A. (2001). Nonlinear finite element methods. *Aerospace Engineering Sciences Department of the University of Colorado. Boulder*.

[3] Drela, M. (1999). Integrated simulation model for preliminary aerodynamic, structural, and control-law design of aircraft. In *40th Structures, Structural Dynamics, and Materials Conference and Exhibit*. p. 1394.

[4] Patil, M. J., Hodges, D. H., and S. Cesnik, C. E. (2000). Nonlinear aeroelastic analysis of complete aircraft in subsonic flow. *Journal of Aircraft*, 37(5), 753–760.

[5] Patil, M. J., Hodges, D. H., and S. Cesnik, C. E. (2001). Nonlinear aeroelasticity and flight dynamics of high-altitude long-endurance aircraft. *Journal of Aircraft*, 38(1), 88–94.

[6] Siqueira, T. M. and Coda, H. B. (2017). Total lagrangian fem formulation for nonlinear dynamics of sliding connections in viscoelastic plane structures and mechanisms. *Finite Elements in Analysis and Design*, 129, 63–77.

[7] Timoshenko, S. P. (1921). On the correction for shear of the differential equation for transverse vibrations of prismatic bars. *Phil. Mag.*, 41, 744–746.

[8] Timoshenko, S. P. (1922). X. on the transverse vibrations of bars of uniform cross-section. *The London, Edinburgh, and Dublin Philosophical Magazine and Journal of Science*, 43(253), 125–131.

[9] Timoshenko, S. P., Goodier, J. N., and Abramson, N. H. (1970). Theory of elasticity. *Journal of Applied Mechanics*, 37, 888.

[10] Timoshenko, S. P. and Gere, J. M. (2009). *Theory of elastic stability*. Courier Corporation.

[11] Bisplinghoff, R. L., Ashley, H., and Halfman, R. L. (2013). *Aeroelasticity*. Courier Corporation.

[12] Bisplinghoff, R. L. and Ashley, H. (1962). *Principles of aeroelasticity*. New York: Wiley & sons.

[13] Wagner, H. (1925). Über die entstehung des dynamischen auftriebes von tragflügeln. *ZAMM-Journal of Applied Mathematics and Mechanics/Zeitschrift für Angewandte Mathematik und Mechanik*, 5(1), 17–35.

[14] Jones, R. T. (1938). Operational treatment of the nonuniform-lift theory in airplane dynamics.

[15] Yates Jr, E. C. (1966). Modified-strip-analysis method for predicting wing flutter at subsonic to hypersonic speeds. *Journal of Aircraft*, 3(1), 25–29.

[16] Silvestre, F. J. and Luckner, R. (2015). Experimental validation of a flight simulation model for slightly flexible aircraft. *AIAA Journal*, 53(12), 3620–3636.

[17] Fung, Y.-c. (1993). *An introduction to the theory of aeroelasticity*. Courier Corporation.

[18] Versiani, T. d. S. S., Silvestre, F. J., Neto, A. B. G., et al. (2019). Gust load alleviation in a flexible smart idealized wing. *Aerospace Science and Technology*, 86, 762–774.

[19] Bruni, C., Cestino, E., Frulla, G., et al. (2014). Development of an aeroelastic wing model with piezoelectric elements for gust load alleviation and energy harvesting. In *ASME 2014 International Mechanical Engineering Congress and Exposition*. American Society of Mechanical Engineers, pp. V001T01A057–V001T01A057.

[20] Pelletier, A. and Mueller, T. J. (2000). Low reynolds number aerodynamics of low-aspect-ratio, thin/flat/cambered-plate wings. *Journal of Aircraft*, 37(5), 825–832.

[21] Newmark, N. M. (1959). A method of computation for structural dynamics. American Society of Civil Engineers.

[22] Duarte Filho, L. A. and Awruch, A. M. (2004). Geometrically nonlinear static and dynamic analysis of shells and plates using the eight-node hexahedral element with one-point quadrature. *Finite Elements in Analysis and Design*, 40(11), 1297–1315.

[23] Urthaler, Y. and Reddy, J. (2005). A corotational finite element formulation for the analysis of planar beams. *Communications in Numerical Methods in Engineering*, 21(10), 553–570.

[24] Nanakorn, P. and Vu, L. (2006). A 2d field-consistent beam element for large displacement analysis using the total lagrangian formulation. *Finite Elements in Analysis and Design*, 42(14-15), 1240–1247.

[25] Simo, J. C. and Vu-Quoc, L. (1986). On the dynamics of flexible beams under large overall motions - the plane case: Part ii. *Journal of applied mechanics*, 53(4), 855–863.

COPYRIGHT STATEMENT

The authors confirm that they, and/or their company or organization, hold copyright on all of the original material included in this paper. The authors also confirm that they have obtained permission, from the copyright holder of any third party material included in this paper, to publish it as part of their paper. The authors confirm that they give permission, or have obtained permission from the copyright holder of this paper, for the publication and distribution of this paper as part of the IFASD-2019 proceedings or as individual off-prints from the proceedings.